Dy3+ doped GeGaSbS fluorescent fiber at 4.4 μm for optical gas sensing: Comparison of simulation and experiment

A. L. Pelé, A. Braud, J. L. Doualan, F. Starecki, Virginie Nazabal, R. Chahal, C. Boussard-Plédel, B. Bureau, R. Moncorgé, P Camy

Dy^{3+} doped GeGaSbS fluorescent fiber at 4.4µm for optical gas sensing: Comparison of simulation and experiment

AL. Pelé[1], A. Braud[1,a)], JL. Doualan[1], F. Starecki[2], V. Nazabal[2], R. Chahal[2], C. Boussard-Plédel[2], B. Bureau[2], R. Moncorgé[1], and P. Camy[1]

[1]*CIMAP - Centre de Recherche sur les Ions, les Matériaux et la Photonique, UMR 6252 CEA-CNRS-ENSICAEN, Université de Caen, France*

[2]*Institut Sciences Chimiques de Rennes, Equipe EVC, UMR-CNRS 6226, Université de Rennes1, Rennes, France*

Abstract

The infrared (IR) fluorescence from Dy^{3+} doped $Ga_5Ge_{20}Sb_{10}S_{65}$ fibers is investigated in details in order to develop bright IR fiber sources emitting at 4.4µm for CO_2 sensing purposes. Optical sensing requires intense IR radiation to probe with accuracy gas concentrations by measuring the gas absorption. We developed a specific modeling describing the Dy^{3+} doped GeGaSbS fiber IR output power by simultaneously solving rate equations and propagation equations within the fibers. This modeling allows the determination of the IR fluorescence guided along the fiber as a function of the Dy^{3+} doping concentration, the propagation losses and the fiber geometry. The results of the simulation are successfully compared with experimental data and are further discussed in order to determine the optimal set of fiber characteristics maximizing the IR fiber output emission.

1. Introduction

Greenhouse gases generated by human activities are known to have a drastic impact on the planet global warming. When averaged over land and ocean surfaces, earth temperature warmed up by 0.85°C from 1880 to 2012 [1]. As a consequence, the necessity to control and measure with precision greenhouse emissions is becoming more and more imperative. Sensors and measurement tools for the control and the monitoring of gaseous pollutants are therefore being developed with a strong emphasis on IR sensors. Indeed, most gases possess absorption bands in the IR range, carbon dioxide (CO_2) having a strong IR absorption in the mid-IR (MIR) at 4.4µm. Optical gas sensors based on optical absorption can bring fast responses with high reactivity, low drifts and a high selectivity. For this type of sensors, rare-earths (RE) doped chalcogenide glasses can be advantageously used as IR light sources operating at room temperature and at lower costs in comparison with quantum cascade Lasers (QCL) which are quite pricy [2-4]. Rare-earths ions doped chalcogenide glasses exhibit quite high absorption and emission cross sections, wide transmission windows expanding to mid-IR wavelengths and very low phonon energies (150–350 cm^{-1}) [5-7]. This low phonon energy leads to a decrease in multi-phonon relaxation rates enabling radiative transitions between RE ions levels in the

[a)]Electronic mail : alain.braud@ensicaen.fr

near and mid-IR ranges. Moreover, RE ions embedded in glasses possess wide emission bands that can be used in differential measurements for the identification of various gases by absorption spectroscopy.

Among the possible rare-earth dopants, Dy^{3+} ions can be used in chalcogenide fibers to identify CO_2 emissions. Dy^{3+} ions hold indeed a MIR emission around 4.4µm ($^6H_{11/2} \rightarrow {}^6H_{13/2}$ transition) which matches the CO_2 absorption wavelength at 4.4µm. When drawn as optical fibers, chalcogenide glasses allow the guiding of the IR fluorescence along the fiber resulting in bright IR light output. A CO_2 gas sensor first prototype including a 4.4µm IR source based on a Dy^{3+} doped Ge-Ga-Sb-S (2S2G) fiber was implemented [5]. After passing through the CO_2 gas cell, the transmitted IR signal is guided by an undoped chalcogenide fiber to an IR detector and the gas concentration is then derived from a differential measurement [5]. In order to further optimize this first CO_2 sensor prototype an optimization of the Dy^{3+} doped 2S2G fiber IR source is crucial. To do so, a model, which encompasses the various spectroscopic and optical properties of Dy^{3+} doped Ge-Ga-Sb-S fibers, is developed to describe the IR fluorescence at 4.4µm and its propagation along the fiber axis, after a laser excitation at 916 nm. The dependence of the IR fluorescence with the fiber length, the propagation losses at the pump and the emission wavelengths, the geometry of the fiber and the doping concentrations are investigated. Experimental data are successfully compared with the simulation results. Thus, the model allows the design of the most efficient RE doped fibers in terms of MIR fluorescence emission for gas sensing.

2. Materials and methods

Dy^{3+} doped core-only chacogenide fibers with the $Ga_5Ge_{20}Sb_{10}S_{65}$ composition were used during the experiments with two Dy^{3+} doping levels: 1000 and 5000ppm. These glasses were prepared by conventional melting and quenching methods [8]. High purity raw materials and purified sulfur were used for the synthesis of glass preforms for fiber drawing. Dy^{3+} doped fibers with a 400µm diameter were obtained by drawing a 10 mm diameter and 10 cm long preform.

The determination of the propagation losses values was determined by the cutback method for two Dy^{3+} doping levels: 1000 and 5000ppm. These attenuation measurements were realized with optical fibers of several meters in length using a Fourier Transform Infrared (FTIR) spectrophotometer Bruker Tensor 37. For each optical fiber length, several measurements were performed and averaged to derive the attenuation values.

The 4.4µm fluorescence dependence with the fiber length was measured by pumping the fiber at 916 nm with a Ti:Sapphire focused on the sample by a 300mm focal length lens. The resulting fluorescence is focused on a Gentec-EO power meter with a 36000 V/W sensitivity with a 25 mm focal length CaF_2 lens. A longwave pass filter with a 3.6 µm cut-off wavelength is placed before the detector to get rid of the residual pump as well as the Dy^{3+} emissions at wavelengths shorter than 4.4µm. It is worth noting that the use of a lens to collect the IR emission from the Dy^{3+} doped fiber is more reliable than placing the power meter directly at the fiber output. Indeed, a direct measurement of the IR power imposes to place the longwave pass filter directly at the fiber output. The remaining pump power is then absorbed by the filter which in turns heats up, giving rise to misleading signals from the IR power meter.

The angular distribution of the 4.4µm fiber emission was measured with a goniometer. A 916 nm Ti:Sapphire pump laser was focused on the Dy^{3+} doped fiber with a 100 mm focal lens. The fiber

output emission at 4.4µm was detected by an InSb photodiode cooled with liquid nitrogen moving from 0° to 180° with respect to the fiber axis, as depicted in figure 1. Three filters at 3.5µm, 3.6 µm and a Si filter were placed in front of the InSb detector to properly reject all parasitic signals. The red part of the set-up is mobile in Figure 1 while elements in black are fixed.

3. Results and discussion

3.1 IR fiber source simulation

3.1.1 IR fiber optical characterization

Propagation losses are among the most important parameters affecting the fiber IR emission. In order to assess the propagation losses, the cut-back method was used for two different doping concentrations of 1000ppm and 5000ppm in Dy^{3+} doped 2S2G fibers as presented in figure 2. From 2 to 5.5µm, the Dy^{3+} doped 1000ppm 2S2G fiber minimum attenuation is in between 0.5 and 0.8 dB/m. Nevertheless, for a doping concentration of 5000ppm, the attenuation rises to 6.5- 8.5 dB/m. This increase with the doping concentration is due to the presence of rare-earths sulfides into the glass, which affect the signal propagation. At 4.3µm, one can observe in Figure 2a) the CO_2 absorption while parasitic absorptions such as SH absorption bands can also be seen.

For the fiber IR output simulation, an average value of propagation losses affecting the Dy^{3+} fluorescence must be derived. This average value is obtained by taking into account the spectral overlap between the Dy^{3+} emission spectrum around 4.4µm and the attenuation spectrum as follows:

$$\bar{\alpha} = \frac{\int \left(I_{Dy}(\lambda) \times \alpha(\lambda) . d\lambda \right)}{\int I_{Dy}(\lambda) . d\lambda} \qquad (1)$$

with $I_{Dy}(\lambda)$ the emission intensity of Dy^{3+} ions around 4.4µm and $\alpha(\lambda)$ the fiber attenuation spectrum (Figure 2b)).
At the pump wavelength of 916 nm, the propagation losses (α_p) were also measured for the two different doping concentrations of 1000ppm and 5000ppm. All attenuation values are summarized in table 1.

3.1.2 fiber IR output modeling

The simulation aims to calculate the power fluorescence emitted at 4.4µm ($^6H_{11/2} \rightarrow {}^6H_{13/2}$ transition) by Dy^{3+} doped 2S2G fibers. The Dy^{3+} ion energy diagram is presented in figure 3. Five relevant levels are considered for the modeling: $^6H_{5/2}$+$^6F_{7/2}$, $^6H_{9/2}$+$^6F_{11/2}$, $^6H_{11/2}$, $^6H_{13/2}$ and $^6H_{15/2}$ named N_4, N_3, N_2, N_1 and N_0, respectively. The transitions depicted by dot-dashed lines represent non-radiative relaxations while solid lines symbolize radiative transitions. The red arrow ($^6H_{15/2} \rightarrow {}^6H_{5/2}$+$^6F_{7/2}$ transition) corresponds to the pump absorption at 916 nm and the $^6H_{11/2} \rightarrow {}^6H_{13/2}$ transition is the fluorescence of interest at 4.4µm between levels 2 and 1. The two main energy transfers taking place between Dy^{3+} ions for the energy levels studied in this work are represented in figure 3 and the corresponding

energy transfer parameters have been calculated using emission lifetimes measurements for different Dy^{3+} concentrations.

The fiber IR output model is based on the simultaneous resolution of the rate equations and the propagation equations describing the evolution of the pump and IR fluorescence powers along the fiber by decomposing the fiber in slices with a dz thickness. In each fiber slice, the IR fluorescence power is calculated by iteration taking into account the pump power and IR fluorescence from the previous slice. The fibers used in the experiment and hence for the simulation have a 350µm diameter; therefore, they are highly multimode and light propagation within these waveguides is governed by geometrical optics laws. Moreover, the pump power density being moderate (maximum of 200W/cm^2) in such fibers, amplified spontaneous emission is negligible. Therefore, the IR fluorescence power emitted by the fiber comes solely from Dy^{3+} ions spontaneous emission. Furthermore, only a fraction η of the IR fluorescence emitted isotropically by Dy^{3+} ions is guided within the fiber and has to be taken into account at each iteration for each fiber slice. This fraction η can be easily calculated by considering the total internal reflection condition for light propagation in the fiber, which is satisfied for all incident angles on the fiber sides above the critical angle θ_c (θ_c =26.4° at 4.4µm in 2S2G glasses). Thus, from this angle, one can derive the solid angle Ω in which the light rays are guided: $\Omega = 2\pi(1 - \cos(\theta))$, where θ is π/2-θ_c = 63.6°. The guided part of the rare-earth ions isotropic emission for each fiber slice is thus $\eta = \Omega/4\pi$ =0.28, when considering only the IR emission tending towards one end of the fiber.

The rate equations are written for the five levels represented in Figure 3. For a pump excitation of 916 nm and fluorescence at 4.4µm, the parameters used for the simulation are summarized in table 2.

The rate equations for the different Dy^{3+} energy levels in steady-state regime are written as:

$^6H_{5/2}+F_{7/2}$

$$\sigma_p . \phi_p . N_0 - \frac{N_4}{\tau_4} = 0 \tag{2}$$

$^6H_{9/2}+F_{11/2}$

$$N_4 . (A_{43}^R + A_4^{MP}) - \frac{N_3}{\tau_3} - W_{30} . N_3 . N_0 = 0 \tag{3}$$

$^6H_{11/2}$

$$N_4 . A_{42}^R + N_3 (A_{32}^R + A_3^{MP}) - \frac{N_2}{\tau_2} - W_{20} . N_2 . N_0 = 0 \tag{4}$$

$^6H_{13/2}$

$$N_4 . A_{41}^R + N_3 . A_{31}^R + N_2 . (A_{21}^R + A_2^{MP}) - \frac{N_1}{\tau_1} + 2 . W_{30} . N_3 . N_0 + 2 . W_{20} . N_2 . N_0 = 0 \tag{5}$$

$$N_T = N_0 + N_1 + N_2 + N_3 + N_4 \tag{6}$$

where N_T is the total Dy^{3+} concentration in the host.

The propagating electromagnetic field is considered as evenly distributed in each fiber slice. Thus, the Dy^{3+} ions are all excited with the same pump power density, regardless of their radial position. The propagation equations for the pump and IR fluorescence powers are then:

$$\frac{dP}{dz} = (-\sigma_p . N_0 - \alpha_p) . P \tag{7}$$

$$\frac{dP_{21}}{dz} = (\sigma_{21} . N_2 - \sigma_{12} . N_1 - \alpha_{21}) . P_{21} + A_{21}^R . \eta . h\nu_{21} . S_f . N_2 \tag{8}$$

where σ_{21} and σ_{12} are the simulated and absorption cross sections respectively ($^6H_{11/2} \rightarrow {}^6H_{13/2}$ transition), $h\nu_{21}$ the photon energy at 4.4µm and α_p and α_{21} the propagation losses at the pump and emission wavelengths respectively (Table 1). The gain term $\sigma_{21} . N_2 - \sigma_{12} . N_1$, which is predominant in doped fibers presenting an amplified spontaneous emission, is very low in our case since the N_1 and N_2 populations are very small due to the weak pump densities (maximum of 200W/cm^2) used in this study. The parameters values used in the modeling are summarized in Table 3. Radiative rates in Table 3 have been derived from a specific Judd-Ofelt analysis for Dy^{3+} doped $Ga_5Ge_{20}Sb_{10}S_{65}$ (2S2G) glasses [5].

One can notice that energy transfer parameters W_{30} and W_{20} are proportional to the Dy^{3+} concentration. This type of dependence is the typical signature of diffusion limited energy transfer processes which can be observed for rather moderate doping levels (below 10000ppm) [9].

3.1.3 Simulation-experiment comparison

The simulation described above enables the calculation of the fiber IR output power at 4.4µm. To confirm the model, IR output power measurements have been performed with 1000ppm and 5000ppm Dy^{3+} doped 2S2G core-only fibers and compared to the simulation values.

Measurements have been done with an initial pump power of 400mW for various fiber lengths. Figure 4 clearly shows the agreement between the measured and simulated power values.

For the 1000ppm Dy^{3+} doped fibers, the 4.4µm fluorescence rises with the fiber length up to a maximum value of 47 µW for a 30 cm fiber length. The 5000ppm Dy^{3+} doped fibers in Fig.4 inset exhibit lower output powers than the 1000ppm fibers for the same fiber lengths. The first reason for this result is the higher propagation losses observed in the 5000ppm Dy^{3+} doped fibers (19dB/m at 916 nm and 20dB/m at 4.4µm) than in the 1000ppm fibers (4dB/m at 916 nm and 1.8dB/m at 4.4µm). Another reason for the lower IR outputs is the occurrence of Dy^{3+} quenched centers in the 5000ppm Dy^{3+} doped fibers explaining the 7% discrepancy found between the modeling results and the experimental data. Unlike the 1000ppm Dy^{3+} doped fibers, the 5000ppm Dy^{3+} doped fibers present an optimal fiber length of 5 cm. For longer fiber lengths, the 4.4µm emission decreases as evidenced in Figure 4 inset. This behavior is mainly due to the large propagation losses at the emission wavelength and will be explained in more details in the following section.

3.2 Model results

3.2.1 Propagation losses influence

In order to illustrate the impact of the propagation losses at the pump and IR fluorescence wavelengths, figure 5 shows the evolution of the IR fluorescence power at 4.4µm as a function of the fiber length taking into account the propagation losses of a Dy^{3+} doped 5000ppm GeGaSbS fiber, pumped at 916 nm. Four curves are presented corresponding to four distinct cases: (a) fiber without any propagation losses, (b) with losses only at the pump wavelength of 916 nm, (c) with losses at the fluorescence wavelength of 4.4µm and (d) with both losses at 916nm and 4.4µm.

In the ideal case of a fiber without propagation losses (a), the IR fluorescence power rises up towards an asymptote. This behavior is simply due to the pump absorption along the fiber following the Beer-Lambert's law. As a consequence, the transmitted pump power decreases exponentially with the fiber length. The pump excites Dy^{3+} ions, which in turns emit at 4.4µm, up to a certain fiber length for which the pump is completely absorbed and no more Dy^{3+} ions are excited. Without any propagation losses (a), the IR signal is guided along the fiber without being affected, even after complete absorption of the pump. As a consequence, the IR output value grows with the fiber length as a cumulative distribution function (Fig.5).

For fibers with propagation losses only at the pump wavelength (case b), one can observe the same behavior as case a). The IR signal still rises with the fiber length since it is not affected by losses during its propagation. However, losses at the pump wavelength induce a decrease in the pump intensity propagating along the fiber. The result is a reduction of the IR power in comparison with curve (a) without any losses.

Curve (c) shows the IR fluorescence evolution when only propagation losses at 4.4µm are taking into account. Unlike the two previous cases, the fluorescence rises up to a maximum for an optimal length of 5.2 cm before decreasing. Like for curve (a), the pump excites Dy^{3+} ions until its complete absorption. But, in this case, the subsequent IR fluorescence is affected by propagation losses at 4.4µm and part of the IR emitted photons is lost while propagating along the fiber. This loss is counterbalanced for short fiber lengths by the strong pump excitation. However, at longer fiber lengths, the pump is completely absorbed and no more IR photons are generated; thus the IR fluorescence starts to decrease.

Finally, curve (d) understandably presents the lowest fluorescence intensity. This IR signal diminution is due both to losses at 916 nm, leading to the reduction of the number of excited Dy^{3+} ions, and to losses at 4.4 µm during the propagation of the IR signal in the fiber.

3.2.2 Doping concentration influence

Figure 6 presents the fluorescence evolution at 4.4µm for four different doping concentrations from 500 to 5000ppm with propagation losses of 4dB/m at 916 nm and 1.8dB/m at 4.4µm. For each curve, a maximum of fluorescence is reached for different optimal lengths before decreasing, in agreement with curve (d) in figure 5. For high Dy^{3+} doping levels, the maximum of fluorescence is achieved for shorter fiber lengths. For instance, at 500ppm, the length given a fluorescence maximum is larger than 40 cm whereas for a 5000ppm doping concentration, the fluorescence maximum is reached for a fiber length of 8 cm. Moreover, the IR fluorescence maximum is higher for high doping levels. In

fact, when the fiber is highly doped, the pump is completely absorbed within a short distance and the IR emitted fluorescence is then little affected by propagation losses at 916 nm and at 4.4µm. On the contrary, for a low doping level, the IR propagation losses impact is larger and thus reduces the maximum IR output value. If we now consider very long fiber lengths up to 50 cm, the fluorescence decreases regardless of the doping concentration because in each case the pump has been entirely absorbed. Thus, the 4.4µm emission tends towards the same value for all doping levels. Another interesting remark in Figure 6 is the fact that the slopes of the various curves at the beginning of the fiber (very short length) directly reflect the doping concentration. Indeed, at the beginning of the fiber, propagation losses are negligible and the IR fluorescence power has a linear dependence with the absorbed pump power while this absorbed pump power is proportional to the doping concentration. As a consequence, the IR fluorescence power is, for instance, ten times higher with 5000ppm than with 500ppm for a given fiber length. However, this proportionality is only valid at the very beginning of the fiber where a linear dependence with the fiber length exists.

3.2.3 Fiber diameter influence

Depending on the fiber diameter, three different pumping regimes affecting the IR output power can be identified: for a quite large diameter, the pump flux is low while for a small diameter, the pump flux is much higher and for an intermediate diameter, the flux is moderate. The IR fluorescence power as a function of the pump power is represented in figure 7 for each fiber diameter considering a 1000ppm Dy^{3+} doped 2S2G fiber with a 23 cm length.

For a 400µm diameter, the fluorescence power changes linearly with the pump power and no saturation is visible. However, for a 40µm diameter, the pump flux becomes significant and leads to a bleaching of the $^6H_{15/2}$ ground state and thus to a saturation effect of the IR emission from the $^6H_{11/2}$ level. Consequently, the fluorescence rapidly reaches a constant value with the input pump power. Finally, for an intermediate diameter of 100µm, one can discern two parts in Fig.7. At low power, the fluorescence changes linearly with the pump power. At higher pump power, a rapid saturation of the IR fluorescence occurs as all Dy^{3+} ions are excited, i.e. the $^6H_{11/2}$ level tends towards a saturation value.

Now, if we study the evolution of the energy level populations as a function of the fiber length in Figure 8, we note that for a 400µm diameter, a 1000ppm doping level and an injected power of 400 mW, the pump flux remains low and the $^6H_{15/2}$ level population is constant and equal to its nominal value regardless of the fiber length L. The IR emitting $^6H_{11/2}$ level population decreases exponentially with the fiber length following the transmitted pump power evolution and thus the Beer-Lambert's law.

On the contrary, for a 40µm fiber diameter, the pump flux is very high and all Dy^{3+} ions are excited. The ground state is bleached and the fiber becomes transparent for a great part of the pump photons. The $^6H_{11/2}$ level remains constant with the fiber length and no longer exhibits a decrease due to the pump absorption. However, one can note a slight increase of the $^6H_{15/2}$ population with L, showing that the ground state bleaching gradually fades away with the fiber length.

Finally, for a 100µm diameter, one can note a partial bleaching of the ground state at the beginning of the fiber, which tends to disappear with the fiber length. As for the $^6H_{11/2}$ level, its population decreases with the fiber length but not as a single exponential.

3.3 IR fiber source angular distribution

The model previously presented clearly describes the mechanisms at play within the Dy^{3+} doped sulfide fibers. However, a complete description of these fibers as IR sources requires the study of the IR output angular distribution. Because of the guiding effect within the fiber, light rays arrive at the output side of the fiber with an incident angle between 0 and 63.6°. Among these rays, only those comprised into a cone with a half apex angle θ_c can be extracted from the fiber, the rest being reflected by total internal reflection. As a consequence, the fiber output power is expected to be evenly distributed over 2π sr. The emission angular distribution at 4.4µm of a typical fiber has been measured and is displayed in figure 9. The black dots represent the measured IR intensity at a given angle θ and the solid line is simply a cosθ function.
The light angular distribution follows, as expected, the cosine emission law $I=I_0.\cos\theta$, as shown in figure 9. Therefore, this IR source can be considered as Lambertian and has the same radiance when viewed from any angle.

4. Conclusion

An IR CO_2 sensor can be advantageously developed using Dy^{3+} doped 2S2G fibers as IR sources. However, an optimization of the Dy^{3+} doped 2S2G fiber IR output power is crucial in order to develop an efficient gas sensor. Thus, we have developed a specific modeling of the 4.4µm IR fluorescence from Dy^{3+} doped GeGaSbS fibers taking into account the different key parameters for this type of light source such as the fiber length, the propagation losses at the pump and the emission wavelengths, the geometry of the fiber and the doping concentration. The comparison between experimental and simulation results clearly shows the validity of the model. This model thus enables us to understand in details the influence of the fiber length, the doping concentration, the propagation losses and the diameter of the fiber in the emitted 4.4µm fluorescence. This modeling points out, in particular, the fact that a higher doping level would allow to obtain larger IR output power provided that propagation losses especially at the emission wavelength are as weak as possible. A rather short fiber, typically around 8cm, could then be used and implemented within a CO_2 IR sensor.

Acknowledgments

This work has been funded by the ADEME STOCKCO2 program within the COPTIK project.

References

1. Intergovernmental Panel on Climate Change (IPPC), “Climate change 2013: The Physical Science Basis,” Cambridge University press (2013)

2. L.B. Shaw, B. Cole, P.A. Thielen, J.S. Sanghera, and I.D. Aggarwal, “Mid-wave IR and long-wave IR laser potential of rare-earth doped chalcogenide glass fiber,” IEEE J. Quantum Electron. 37(9), 1127-1137 (2001).

3. T. Schweizer, B.N. Samson, R.C. Moore, D.W. Hewak, and D.N. Payne, “Rare-earth doped chalcogenide glass fiber laser,” Electron. Lett. 33(5), 414-416 (1997).

4. B.J. Park, H.S. Seo, J.T. Ahn, Y.G. Choi, J.Heo, and J. Chung, (Dy(3+) doped Ge-Ga-Sb-Se glasses and optical fibers for the mid-IR gain media,” J. Ceram. Soc. Jpn. 116(1358), 1087-1091 (2008).

5. F. Starecki, F. Charpentier, J.-L. Doualan, L. Quetel, K. Michel, R. Chahal, J. Troles, B. Bureau, A. Braud, P. Camy, V. Moizan, and V. Nazabal, “Mid-IR optical sensor for CO2 detection based on fluorescence absorbance of Dy^{3+}:$Ga_5Ge_{20}Sb_{10}S_{65}$ fibers,” Sensors & Actuators: B. Chemical, **207,** (2015) 518–525.

6. F. Charpentier, F. Starecki, J. L. Doualan, P. Jóvári, P. Camy, J. Troles, S. Belin, B. Bureau, and V. Nazabal, “Mid-IR luminescence of Dy^{3+} and Pr^{3+} doped $Ga_5Ge_{20}Sb_{10}S(Se)_{65}$ bulk glasses and fibers”, Mat. Letters **101**, 21 (2013).

7. F. Charpentier, V. Nazabal, J. Troles, Q. Coulombier, L. Brilland, C. Boussard-Pledel, P. Nemec, H. Lhermite, J. Charrier, F. Smektala, M. Frumar, K. Le Pierres, N.Thybaud, B. Bureau, F. Baldini, and J. Homola, ”Infrared optical sensor for CO2 detection” , R.A. Lieberman (Eds.) Optical Sensors, 735610 (2009).
8. J. Kobelke, J. Kirchhof, K. Schuster, and A. Schwuchow, “Effects of carbon, hydrocarbon and hydroxide impurities on praseodymium doped arsenic sulfide based glasses,” J. Non-Cryst. Solids 284(1-3), 123-127 (2001).

9. M.J. Weber, «Luminescence decay by Energy Migration and Transfer: Observation of Diffusion-Limited Relaxation» *Physical Review B,* vol. 4 (1971)

Figure captions

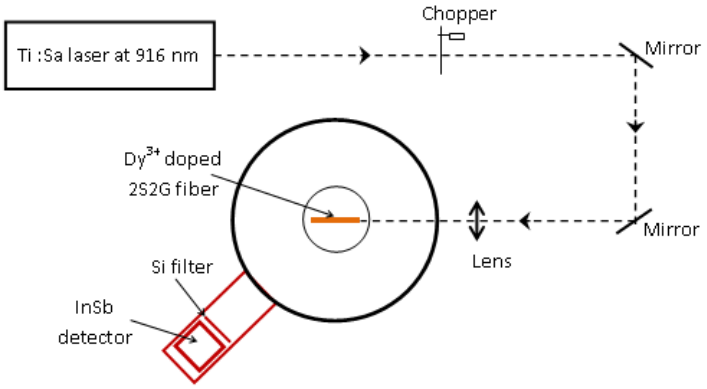

Fig. 1 - Angular distribution measurement set-up .

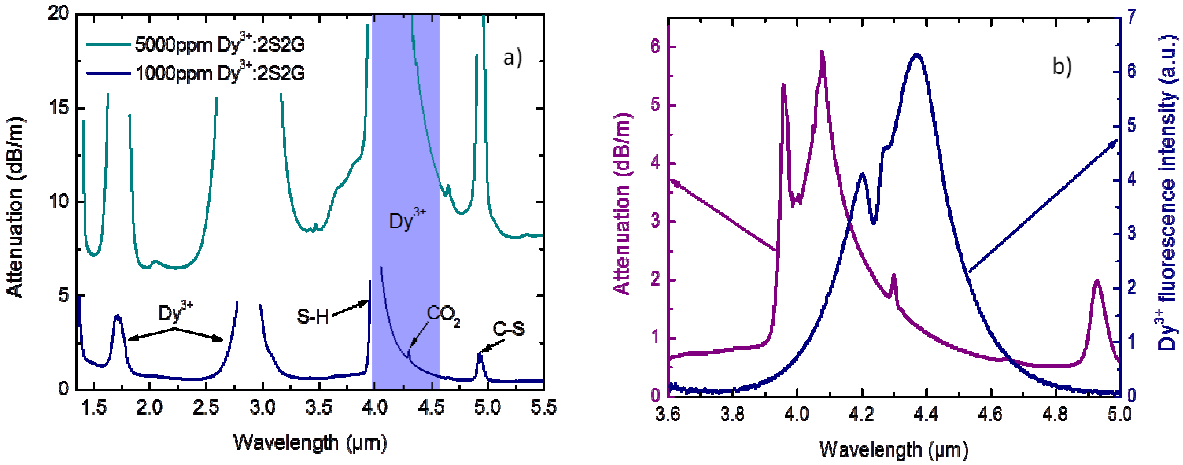

Fig. 2 – a) Attenuation curves of core-only Dy^{3+} doped 1000ppm and 5000ppm 2S2G fibers. The blue zone corresponds to the Dy^{3+} emission around 4.4µm. b) Spectral overlap between the Dy^{3+} emission spectrum around 4.4µm and the fiber attenuation spectrum.

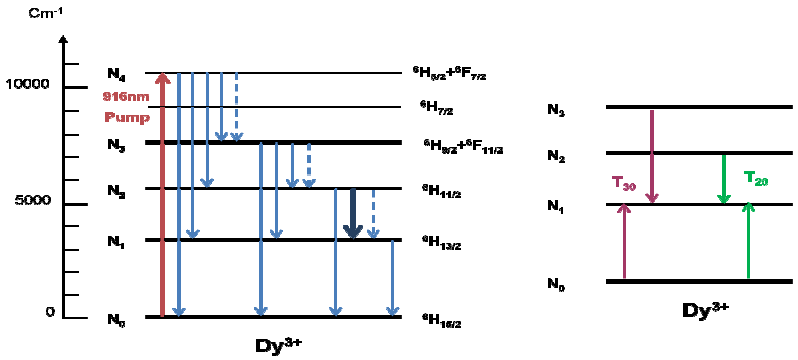

Fig. 3 - Dy^{3+} energy level diagram and emission at 4.4µm resulting of the pumping at 916nm and energy transfers taking place among Dy^{3+} ions

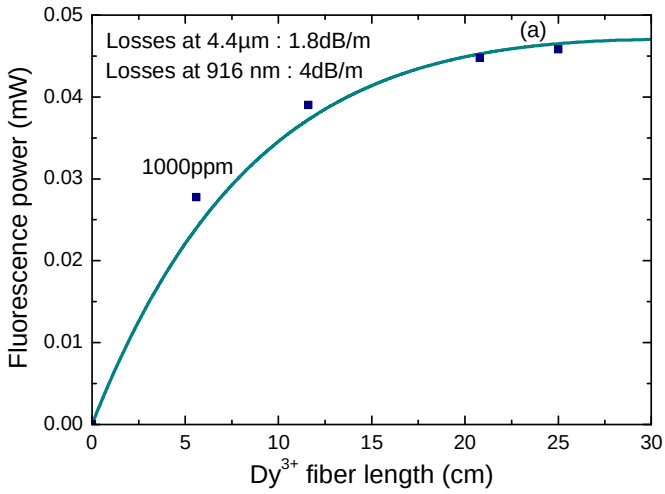

Fig. 4 – Experimental (dots) and simulation (solid lines) results for the 4.4µm output power as a function of the fiber length for two doping levels: 1000 and 5000ppm (inset).

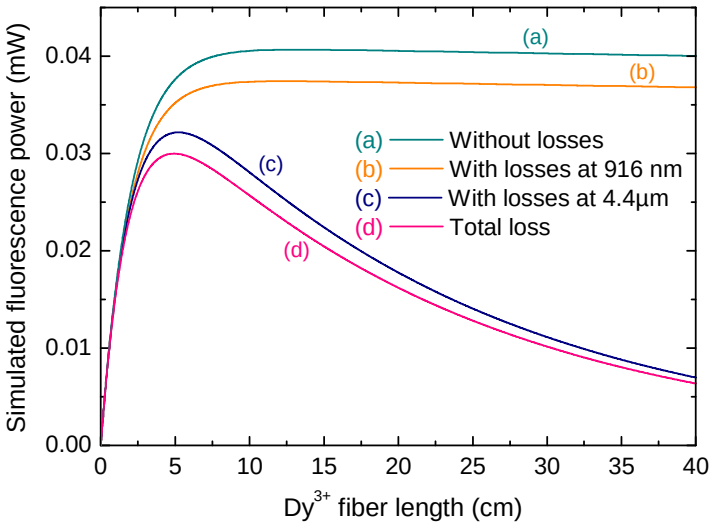

Fig. 5 - IR Fluorescence intensity as a function of the Dy^{3+} fiber length and with propagation losses of 19dB/m at 916 nm and 20dB/m at 4.4µm.

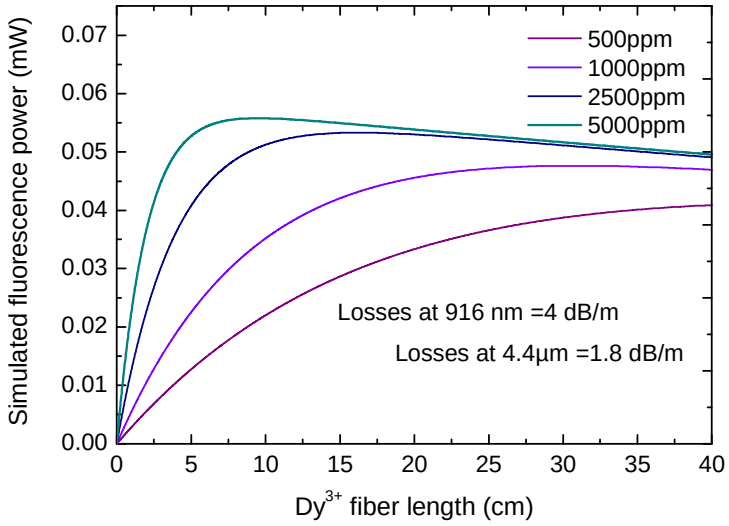

Fig. 6 - IR output power as a function of the Dy^{3+} fiber length and for various doping concentrations.

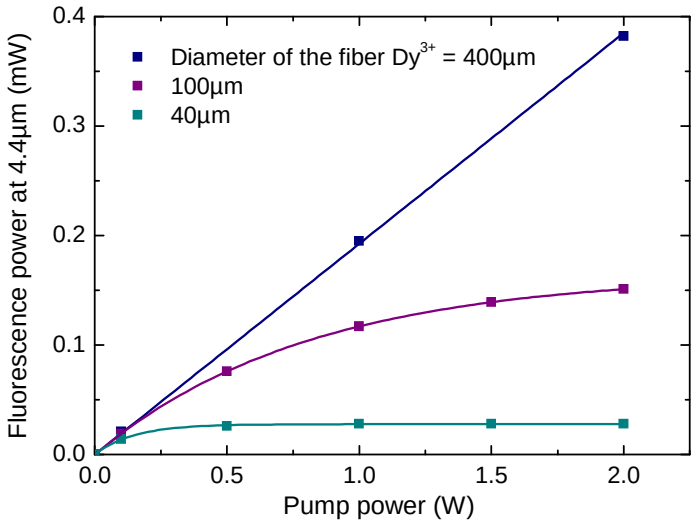

Fig.7 – IR output power at 4.4µm as a function of the input pump power for different fiber diameters and a length of 23 cm.

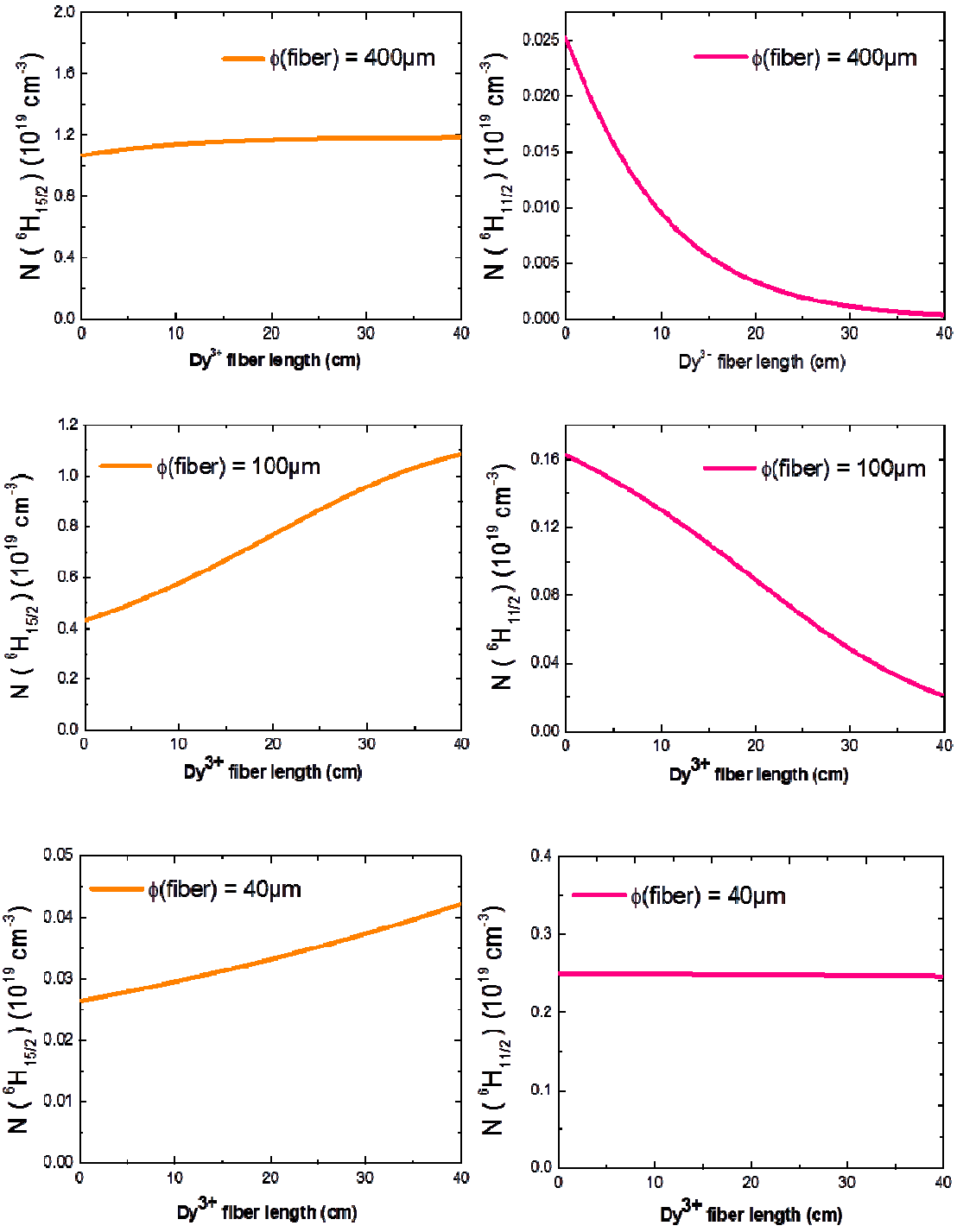

Fig. 8 –Dy^{3+} $^6H_{15/2}$ and $^6H_{11/2}$ levels populations as a function of the fiber length and for several fiber diameters (400 mW incident pump power and a 1000ppm doping concentration).

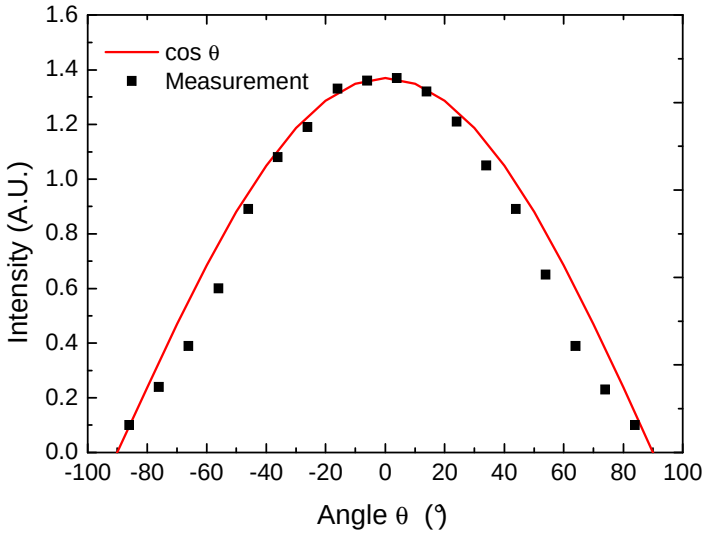

Fig.9 - Angular distribution of the IR output of a 5000ppm Dy^{3+} doped 2S2G fiber.